

# A new astrophysical solution to the Too Big To Fail problem

## Insights from the MoRIA simulations

R. Verbeke<sup>1</sup>, E. Papastergis<sup>2\*</sup>, A.A. Ponomareva<sup>3,2</sup>, S. Rath<sup>1,4</sup>, and S. De Rijcke<sup>1</sup>

<sup>1</sup> Astronomical Observatory, Ghent University, Krijgslaan 281, S9, 9000 Gent, Belgium  
e-mail: [robbert.verbeke@ugent.be](mailto:robbert.verbeke@ugent.be), [sven.derijcke@ugent.be](mailto:sven.derijcke@ugent.be)

<sup>2</sup> Kapteyn Astronomical Institute, University of Groningen, Landlevan 12, 9747AD Groningen, The Netherlands  
e-mail: [papastergis@astro.rug.nl](mailto:papastergis@astro.rug.nl), [ponomareva@astro.rug.nl](mailto:ponomareva@astro.rug.nl)

<sup>3</sup> Research School of Astronomy & Astrophysics, Australian National University, Canberra, ACT 2611, Australia

<sup>4</sup> IIT Roorkee, Haridwar Highway, Roorkee, Uttarakhand 247667, India

Received date; Accepted date

### ABSTRACT

**Aims.** We test whether advanced galaxy models and analysis techniques of simulations can alleviate the Too Big To Fail problem (TBTf) for late-type galaxies, which states that isolated dwarf galaxy kinematics imply that dwarfs live in lower-mass halos than is expected in a  $\Lambda$ CDM universe. Furthermore, we want to explain this apparent tension between theory and observations.

**Methods.** To do this, we use the MoRIA suite of dwarf galaxy simulations to investigate whether observational effects are involved in TBTf for late-type field dwarf galaxies. To this end, we create synthetic radio data cubes of the simulated MoRIA galaxies and analyse their H I kinematics as if they were real, observed galaxies.

**Results.** We find that for low-mass galaxies, the circular velocity profile inferred from the H I kinematics often underestimates the true circular velocity profile, as derived directly from the enclosed mass. Fitting the H I kinematics of MoRIA dwarfs with a theoretical halo profile results in a systematic underestimate of the mass of their host halos. We attribute this effect to the fact that the interstellar medium of a low-mass late-type dwarf is continuously stirred by supernova explosions into a vertically puffed-up, turbulent state to the extent that the rotation velocity of the gas is simply no longer a good tracer of the underlying gravitational force field. If this holds true for real dwarf galaxies as well, it implies that they inhabit more massive dark matter halos than would be inferred from their kinematics, solving TBTf for late-type field dwarf galaxies.

**Key words.** galaxies: dwarf – galaxies: kinematics and dynamics – galaxies: structure – methods: numerical – (cosmology:) dark matter

## 1. Introduction

$\Lambda$ CDM, generally considered as the current standard model for cosmology and cosmic structure formation, is a superbly successful theory on large, super-galactic distance scales (Mamon et al. 2017; Rodríguez-Puebla et al. 2016; Planck Collaboration et al. 2016; Cai et al. 2014; Suzuki et al. 2012). However, going to smaller, sub-galactic scales, and especially in the regime of dwarf galaxies,  $\Lambda$ CDM encounters a number of persistent problems.

One such problem is called Too Big Too Fail, or TBTf, first formulated in the context of the Local Group. Given the many factors that suppress star formation in dwarf galaxies, such as supernova feedback and the cosmic UV background, visible dwarf galaxies are expected to reside in relatively scarce high- $v_{\text{circ}}$  dark-matter halos. This would also agree with their small observed number density. However, most observed Milky Way satellites have circular velocities  $v_{\text{circ}} < 30 \text{ km s}^{-1}$ , estimated from their stellar kinematics, indicating that these satellites seem to live in low- $v_{\text{circ}}$  subhalos, which are too abundant in comparison with the observed number of Milky Way satellites (Boylan-

Kolchin et al. 2011, 2012). The TBTf problem is also present for the satellite system of Andromeda (Tollerud et al. 2014) and for field dwarfs in the Local Group and Local Volume (e.g. Ferrero et al. 2012; Garrison-Kimmel et al. 2014; Papastergis et al. 2015).

Several possible solutions to this problem have been suggested. For example, if the Milky Way were to have a smaller virial mass, then it would also host a smaller number of massive subhalos (Wang et al. 2012). Another way out is to take into account the fact that baryonic processes, such as supernova feedback, can flatten the inner dark-matter density distribution, converting a high- $v_{\text{circ}}$  cuspy density profile into a low- $v_{\text{circ}}$  cored one at constant halo mass. By fitting the mass-dependent DC14 profile (Di Cintio et al. 2014) to the kinematical data of the Local Group dwarf galaxies, Brook & Di Cintio (2015) found that dwarf galaxies inhabit more massive halos than previously thought, thus alleviating the TBTf problem. Other effects that help reduce dwarf galaxy circular velocities in the context of the Local Group include tidal stripping (Sawala et al. 2016).

In their analysis of the TBTf problem in field dwarfs, where only internal baryonic effects can be invoked to reduce halo circular velocities, (Papastergis & Shankar 2016,

\* NOVA postdoctoral fellow

henceforth referred to as P16) use abundance matching to derive the relation between the observed H I rotation velocity inferred from the galaxy 21cm emission line profile,  $W_{50}$ , and the maximum halo circular velocity  $v_{h,\max}$  such that the halo velocity function (VF) found in simulations (Sawala et al. 2015) corresponds to the observed field galaxy VF (Haynes et al. 2011; Klypin et al. 2015). Hereafter, we will refer to this relation between  $W_{50}$  and  $v_{h,\max}$  as the P16-relation. Then, these authors fit NFW (Navarro et al. 1996) and DC14 profiles to the outer-most datapoint of the rotation curves of a set of field dwarf galaxies to infer their  $v_{h,\max}$ . This allows them to put individual  $v_{\text{rot,H I}} - v_{h,\max}$  datapoints on the inferred statistical relation. As these authors note: “ $\Lambda$ CDM can be considered successful only if the position of individual galaxies on the  $W_{50} - v_{h,\max}$  plane is consistent with the relation needed to reproduce the measured VF of galaxies.”. As it turns out, the individual galaxies are not consistent with the expected P16-relation.

The discrepancy between these results and those from Brook & Di Cintio (2015) results from the radius at which the circular velocity is measured: for measurements beyond the core radius ( $\gtrsim 2\text{kpc}$ ), fitting a DC14 profile gives similar results as using a cusped NFW profile. The TBTF problem can therefore not be (fully) explained by core creation alone (see also Papastergis & Ponomareva 2016).

For the present paper, we take to heart the message from P16: if  $\Lambda$ CDM is correct, then late-type field dwarfs should have higher circular velocities than is estimated from their H I kinematics. In order to investigate such a possible mismatch between the maximum circular velocity as inferred from gas kinematics and its actual value, we perform H I observations of a set of simulated dwarf galaxies. In Sect. 2, we briefly present the MoRIA simulations and the procedure to construct and analyse mock H I data-cubes. In Sect. 3, we fit a halo profile to the outermost datapoint of the rotation curves of the simulated galaxies and compare with the results of P16. In Sect. 4 we give some possible explanation for these results. Our conclusions are presented in Sect. 5.

For clarity, we define the different types of velocities used throughout this paper here:

- $v_{\text{rot,H I}}(R)$   
the mean tangential velocity of the H I gas at a radius  $R$  from the galaxy center. This can be determined from observations by fitting a tilted-ring model to the H I velocity field or the full data-cube.
- $v_{\text{circ}}^{\text{obs}}(R)$   
the circular velocity derived from the  $v_{\text{rot,H I}}(R)$  profile by correcting for asymmetric drift (see Sect. 2.4).
- $v_h^{\text{true}}(R)$   
the “true” circular velocity profile, inferred from the total enclosed mass profile  $M(R)$  as

$$v_h^{\text{true}}(R) = \sqrt{\frac{GM(R)}{R}}. \quad (1)$$

- $v_{\text{out,H I}} = v_{\text{circ}}^{\text{obs}}(R_{\text{out}})$   
the outermost value of the rotation curve.
- $v_{h,\max}^{\text{true}} = \max(v_h^{\text{true}})$   
the maximum circular halo velocity.
- $v_{h,\max}^{\text{fit}}$ ,  $v_{h,\max}^{\text{NFW}}$ , or  $v_{h,\max}^{\text{DC14}}$   
the maximum circular velocity obtained by fitting an NFW or DC14 profile to  $v_{\text{out,H I}}$ . Denoted by  $v_{h,\max}^{\text{fit}}$  in general and  $v_{h,\max}^{\text{NFW}}$  or  $v_{h,\max}^{\text{DC14}}$  when the halo profile is specified.

- $W_{50}$

The FWHM of the galactic 21cm emission line profile, corrected for inclination to an edge-on view. .

All except for  $W_{50}$  refer to a spatially resolved kinematic measurement or calculation.  $W_{50}$  on the other hand is derived from the spatially unresolved H I spectrum. Since  $W_{50}$  does not correspond to any specific radius, it does not generally contain enough information to estimate the mass of the host halo by fitting a certain mass profile. However,  $W_{50}$  measurements exists for large samples of galaxies, which allows for an accurate measurement of the number density of galaxies as a function of  $W_{50}$ , i.e. the VF.

## 2. The MoRIA simulations

We use the MoRIA (Models of Realistic dwarfs In Action) suite of  $N$ -body/SPH simulations of late-type isolated dwarf galaxies. Details concerning the setup and subgrid physics model of these simulations can be found in Verbeke et al. (2015, V15). Since this paper, more simulations were run with different masses and merger histories, but the conclusions presented in V15 still stand. At the moment of writing, MoRIA consists of  $\sim 30$  dwarf galaxy simulations, of which we will discuss 10 in more detail.

It is important to note that the atomic hydrogen density of every gas particle has already been computed, based on its density, temperature, composition, and incident radiation field, to be used in the subgrid model of the MoRIA simulations, as described in De Rijcke et al. (2013). Thus, all H I observables we describe below derive directly from the simulations without any extra assumptions or approximations.

### 2.1. H I disk sizes and flattening

We aim to investigate H I rotation curves, with strong focus on the outer-most data point. It is therefore very important that the simulated dwarf galaxies have realistic H I disk sizes and shapes. In V15, we already showed that the MoRIA dwarfs have an atomic interstellar medium (ISM) with realistic spatial substructure, as quantified by the H I power spectrum.

Here, we also investigate the flattening and size of the H I disks. For this, we produce H I surface density contour maps of the H I and fit ellipses to the contour corresponding to a column density of  $\Sigma_{\text{H I}} = 1 \text{ M}_{\odot} \text{ pc}^{-2} \approx 1.25 \times 10^{20} m_{\text{H}} \text{ cm}^{-2}$ . We do this for different orientations and take the minimum value of the flattening  $q$ , defined as the ratio of the minor and major axis of the ellipse.  $q$  is thus the intrinsic axis ratio of the galaxy. The frequency distribution of the axis ratio  $q$  of the simulated MoRIA galaxies is shown in Fig. 1, along with that of observed dwarf galaxies, derived by Roychowdhury et al. (2010) for the FIGGS sample of faint galaxies. In Fig. 2, we show the total H I mass, denoted by  $M_{\text{H I}}$ , in function of the disk size,  $R_{\text{out}}$ , both for simulated and observed galaxies. The disk size is defined as the major axis of the elliptical contour corresponding to a column density of  $\Sigma_{\text{H I}} = 1 \text{ M}_{\odot} \text{ pc}^{-2}$ .

We generally find good agreement with the observed flattening distribution although the MoRIA dwarfs appear to have slightly thicker H I disks than the observed dwarfs. However, the MoRIA dwarfs were not intended to be equivalent to the FIGGS sample. Indeed, most of the FIGGS

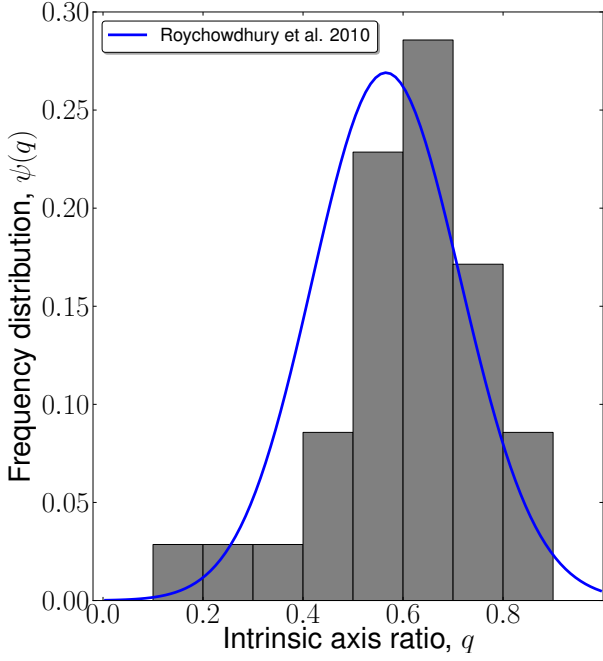


**Fig. 1.** Histogram of the axis ratios of the MORIA dwarf galaxies versus the frequency distribution obtained by Roychowdhury et al. (2010) for the FIGGS galaxies.

galaxies have  $M_{\text{HI}} \sim 10^7 - 10^9 M_\odot$  (Fig. 1c in Begum et al. 2008b) whereas the MORIA dwarfs more cover the  $M_{\text{HI}} \sim 10^6 - 10^7$  regime. Roychowdhury et al. (2010) also note that galaxies with high inclinations may be overrepresented in their sample which might lead to a slight underestimate for the mean intrinsic axis ratio  $\langle q \rangle$ . Furthermore, they assumed in their analysis that the gas disks are oblate spheroids, and showed that  $\langle q \rangle$  would be higher when assuming a prolate spheroid. Galaxies are not necessarily oblate spheroids (e.g. Cloet-Osselaer et al. 2014), so the real  $\langle q \rangle$  might be higher. Considering all this, it is remarkable that we find a distribution that looks so similar to the observed one.

As can be seen in Fig. 2, the sizes of the HI disks of the MORIA dwarfs are realistic as well: they follow the same mass-size relation and FWHM-size relation as the observed galaxies compiled in P16. This is of crucial importance because it determines the position of the outermost datapoint to which the circular velocity profile is fitted in order to estimate  $v_{h,\text{max}}^{\text{fit}}$ .

## 2.2. Mock data cubes

The procedure to produce a cube of 21cm data for a MORIA dwarf is as follows. First, we tilt the galaxy such that its angular momentum vector is inclined by  $45^\circ$  with the line of sight. Then, the mass of each gas particle is assigned to a cell in a three dimensional grid based on its projected position and its line-of-sight velocity. The velocity grid is chosen with a resolution of  $2.5 \text{ km s}^{-1}$ . To account for thermal broadening, the HI mass of each gas particle is smeared out over neighboring velocity channels using a Gaussian with a dispersion given by

$$\sigma_{\text{TB}} = \sqrt{\frac{kT}{m_p}}, \quad (2)$$

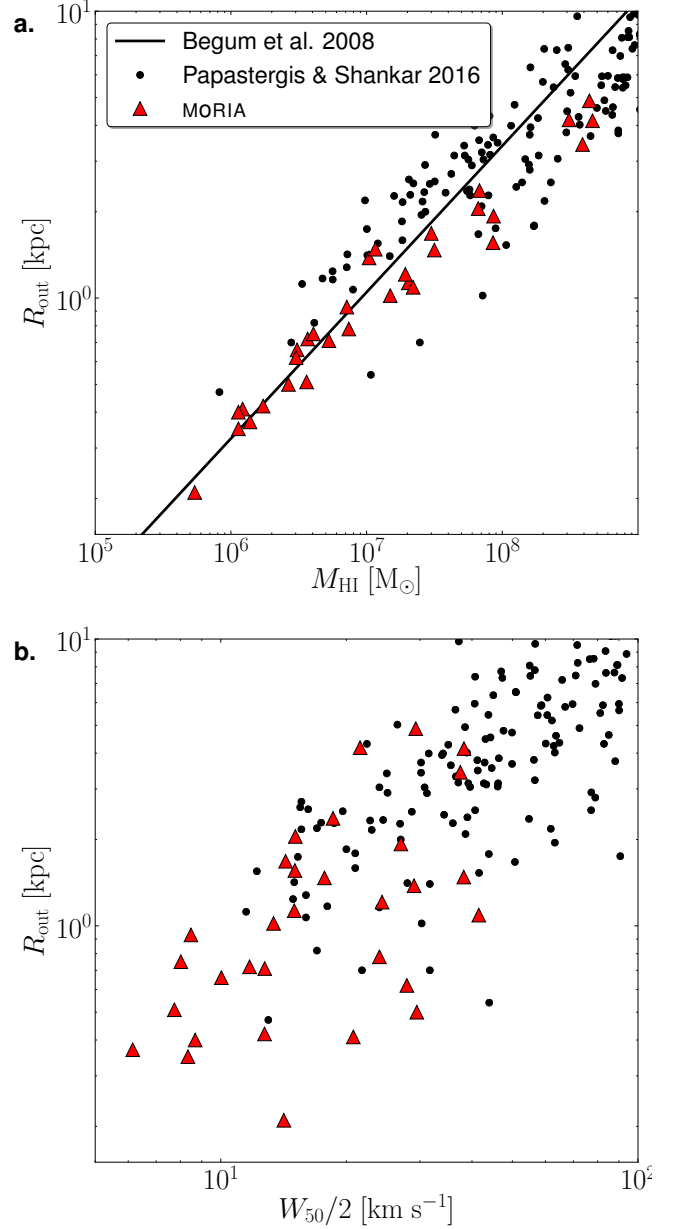


**Fig. 2.** **a.** Atomic gas mass,  $M_{\text{HI}}$  versus H I disk size,  $R_{\text{out}}$ , and **b.**  $W_{50}/2$  versus  $R_{\text{out}}$  of the MORIA dwarfs (in red) versus observations compiled in P16. For the simulations,  $R_{\text{out}}$  is the semi-major axis of the best fitted ellipse to the contour with  $\Sigma_{\text{HI}} = 1 M_\odot \text{ pc}^{-2}$ . The relation in panel **a.** is the one found for the FIGGS sample at  $1 M_\odot \text{ pc}^{-2}$  ( $\log(M_{\text{HI}}) = 1.96 \log(2R_{\text{out}}) + 6.37$ ; Begum et al. 2008a).

where  $T$  is the temperature of the particle,  $k$  is the Boltzmann constant and  $m_p$  the mass of a proton. The gas is allowed to cool down to  $T = 10 \text{ K}$  while it becomes fully ionized around  $T \sim 10^4 \text{ K}$  so the thermal broadening achieves values in the interval  $0.29 \text{ km s}^{-1} \lesssim \sigma_{\text{TB}} \lesssim 10 \text{ km s}^{-1}$ . Finally, each velocity channel is convolved with a Gaussian beam profile as well. The full width at half the maximum (FWHM) of the beams are shown in the top left panels in Figs. 3 and A.1-A.5. The beam size was chosen so that it fits at least 10 times within the HI radius of the galaxy. For

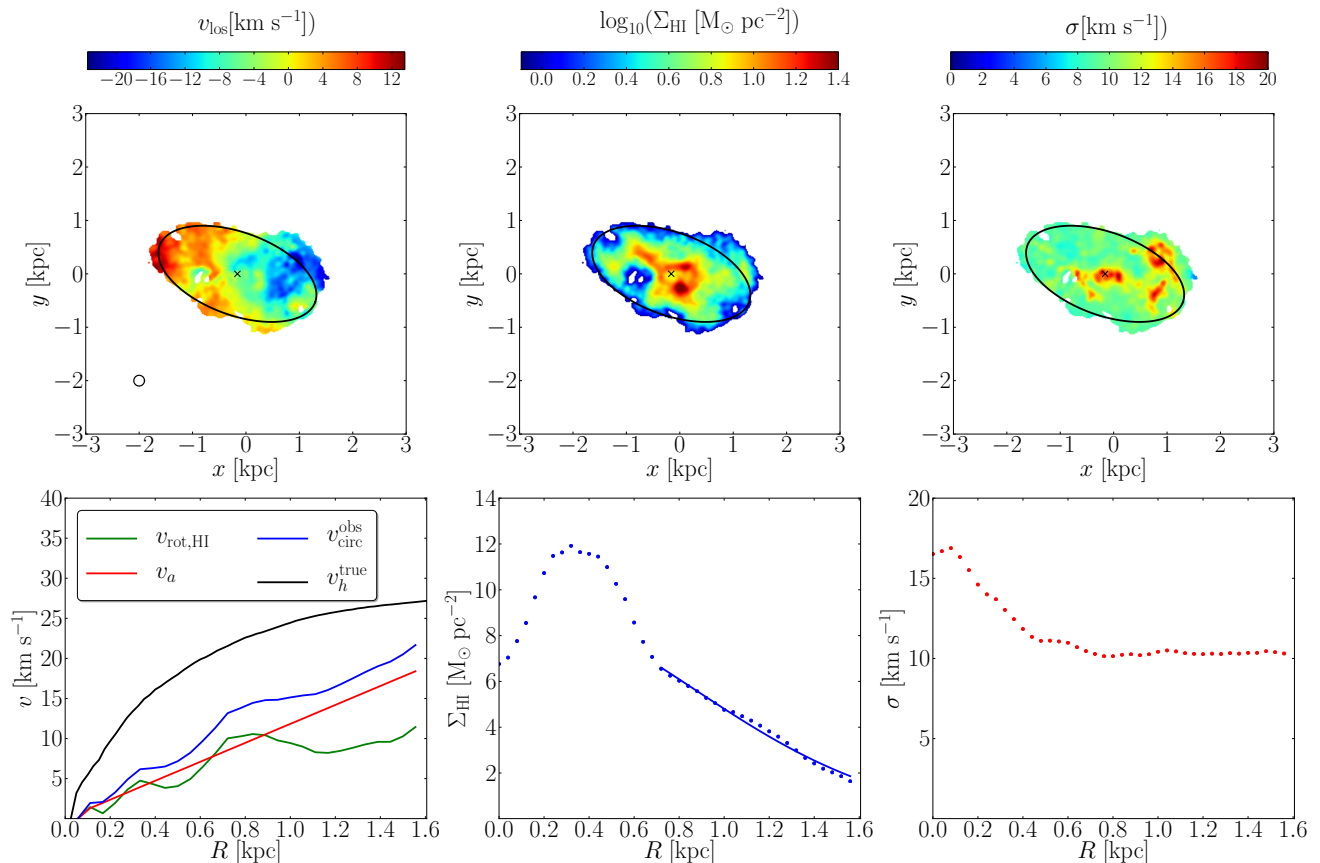


**Fig. 3.** **Top panels:** velocity field (*left*), density (middle) and dispersion (right) map of one simulated galaxy. The beam size used is shown in the top left panel. **Bottom panels:** The rotation curves, with the rotational velocity obtained using tilted ring fitting in GIPSY in green, correction for pressure support in red, full circular velocity in blue and theoretical halo velocity in black (*left*), H I density profile, with the fit necessary for the pressure support correction plotted as a solid line shown over the area that was used for the fit (*middle*), H I velocity dispersion profile (*right*). The other MORIA galaxies are shown in Appendix A.

the simulations presented here, this comes down to 100 pc for the ones with  $R_{\text{out}} \sim 1$  kpc. (Figs 3, A.1 and A.2) and 200 pc for the larger ones (Figs. A.3-A.5). The resolution of the spatial grid is chosen so that the beam size corresponds to 5 pixels.

This three-dimensional mass grid is then saved in the FITS format.

### 2.3. Rotation curves

We opt for two analysis codes to derive rotation curves for the MORIA dwarfs based on their radio data cubes: GIPSY (The Groningen Image Processing SYstem; van der Hulst et al. 1992) and <sup>3D</sup>Barolo (Di Teodoro & Fraternali 2015). GIPSY has a built-in routine, ROTCUR, which fits a tilted-ring model to H I velocity field (Begeman 1989). Of the full suite of MORIA dwarfs, ten have velocity fields and shapes that are sufficiently relaxed to be amenable to analysis with ROTCUR. The ones that were not selected had a very irregular H I morphology or velocity field. <sup>3D</sup>Barolo fits a model directly to the full data-cube, which makes it useful for a comparison with the GIPSY results. The tilted-ring model in <sup>3D</sup>Barolo is populated with gas clouds at random spatial positions. This feature makes this code very useful for determining the kinematics of dwarf galaxies with sometimes highly disturbed gas distributions.

Ideally, given the way we produce the datacubes, one would expect the center of each ring in the tilted-ring model to coincide with the nominal galaxy center grid, its inclination to be 45°, and its position angle (PA) to be 90°. However, strongly disturbed and warped disks can lead to tilted-ring models with the apparent ring centers, inclinations, and PAs significantly shifted away from their expected values. The parameters are chosen by fitting an ellipse to the isodensity contour of  $\Sigma_{\text{HI}} = 1 \text{ M}_{\odot} \text{pc}^{-2}$ . These were checked and adjusted so that, for instance, the rotation would be around the minor axis. The inclination is typically chosen to its true value of 45° unless the shape of the galaxy clearly implies a different inclination. The chosen ellipses are shown in the top panels of Figs. 3 and A.1-A.5. The systematic velocity is chosen as roughly the value of the center (typically close to 0 km s<sup>-1</sup>). We keep these values fixed for each radius. The rotational velocity is thus the only parameter that is fitted.

### 2.4. Pressure support corrections

In the low-mass systems under investigation here, pressure support is expected to be significant, entailing a sizable correction for pressure support. For the latter, we follow the approach typically used in observational studies of dwarf kinematics (Lelli et al. 2012). The pressure support correc-



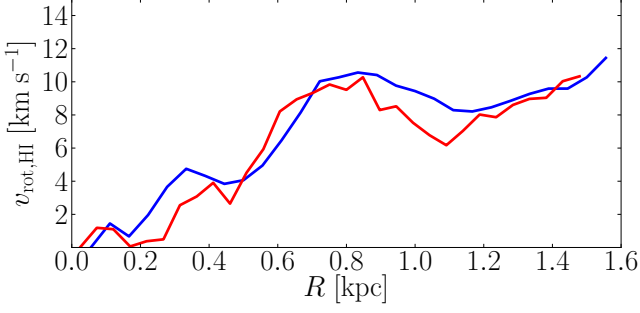


**Fig. 4.** Rotation curves of one of the MORIA dwarfs, obtained using GIPSY (in blue) and using <sup>3D</sup>Barolo (in red). The simulation is the one shown in Fig. 3.

tion is given by

$$v_a^2(R) = -\sigma^2 \frac{\partial \ln(\sigma^2 \Sigma_{H I})}{\partial \ln R}, \quad (3)$$

where  $\sigma$  is the velocity dispersion and  $\Sigma_{H I}$  is the intrinsic gas surface density. We assume a prescription for  $\Sigma_{H I}$  of the form

$$\Sigma_{H I}(R) = \Sigma_0 \exp(-R^2/2s^2), \quad (4)$$

with  $s$  a radial scale length. Since we are only interested in  $v_{out}$ , the fit is performed for the outer regions and the velocity dispersion is assumed constant at the value at the outer edge of the galaxy. This is justified since the radial variation of  $\sigma$  is typically small. The pressure support correction then becomes

$$v_a^2(R) = \sigma_{out}^2 \frac{R^2}{s^2}. \quad (5)$$

Given the rotation velocity  $v_{rot}$  provided by the tilted-ring fit and the pressure support correction  $v_a$ , we obtain an estimate for the true circular velocity as

$$v_{circ}^{obs}(R) = \sqrt{v_{rot,H I}^2(R) + v_a^2(R)}. \quad (6)$$

The obtained rotation curves are shown in the lower left panels of Fig. 3. In this Fig., we show the three first moment maps of the data cube, the rotation and circular velocity curves, the radial H I density profile, and the H I velocity dispersion profile. In the density profile diagram, the region where the parameters of the pressure support model have been determined is indicated. In this region, the pressure support correction can be computed relatively reliably; at smaller radii, the resulting pressure support correction should be taken with a grain of salt.

In Fig. 4, we compare rotation curves determined with GIPSY and with <sup>3D</sup>Barolo. For the tilted-ring analysis with <sup>3D</sup>Barolo, we used 20 rings, each with a radial size of  $10\text{arcsec} \approx 50\text{parsec}$ . We keep all parameters the same as in the analysis with GIPSY, with the exception of an additional free parameter of scale height, while fitting the rotational velocity. We notice from the channel maps, two of which are shown in Fig. 5, that our observed simulations (in blue) and the model (in red) tally quite well. Overall, the agreement between the results obtained with both codes is satisfactory, especially in the outer regions which are of greatest interest to us.

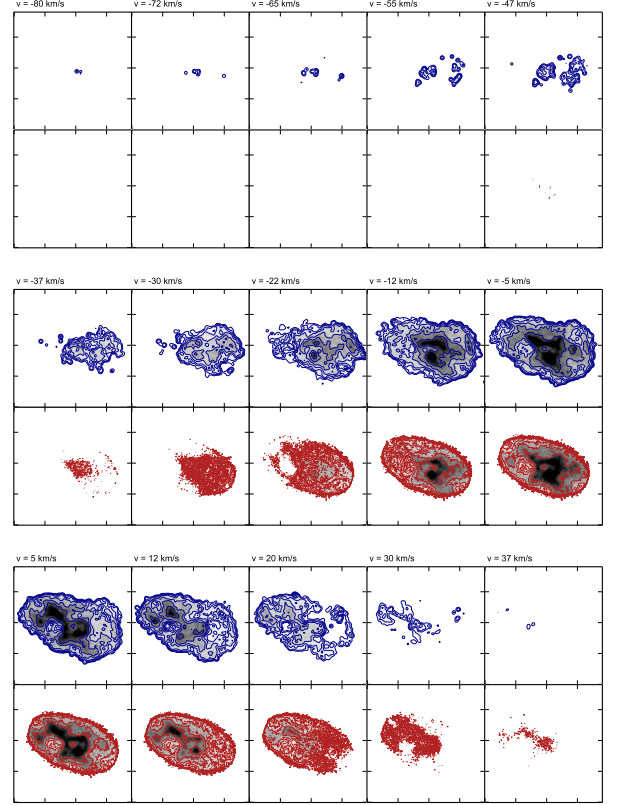


**Fig. 5.** Channel maps of one of the MORIA dwarfs, in blue, and the model fit with <sup>3D</sup>Barolo, in red. The <sup>3D</sup>Barolo model reproduces the most salient features of the input data cubes. The simulation is the one shown in Fig. 3.

### 3. Results

#### 3.1. The $W_{50} - v_{h,max}$ relation

In their study of the TBTF problem in field dwarfs, P16 derived the average relation between the observed H I velocity width of galaxies,  $W_{50}$ , and the maximum circular velocity of their host halos,  $v_{h,max}^{true}$ , such that the observed VF of galaxies (Haynes et al. 2011; Klypin et al. 2015, P16) can be reproduced within the  $\Lambda$ CDM cosmological model. The observed rotation velocity used here is  $W_{50}/2$ . Here, we check where the MORIA dwarfs fall in the  $W_{50} - v_{h,max}^{true}$  plane.

Figure 6 shows the location of the MORIA dwarfs in the  $W_{50} - v_{h,max}^{true}$  plane. The MORIA dwarfs follow very well the average relation derived in P16, a fact that ensures that MORIA dwarfs are produced at the correct number densities as a function of their  $W_{50}$  (i.e., the MORIA simulation reproduces the observational VF). Similar results were also obtained by Macciò et al. (2016) based on the NIHAO hydrodynamical simulations (Wang et al. 2015) and Brooks et al. (2017) based on a set of hydrodynamic simulations of galaxy formation carried out by Governato et al. (2012), Brooks & Zolotov (2014) and Christensen et al. (2014).

However, reproducing the observational VF alone does not necessarily mean that the cosmological problems faced by  $\Lambda$ CDM on small scales have been resolved. In particular, a successful simulation must also be able to reproduce the internal, spatially-resolved, kinematics of observed dwarfs. This is a crucial point, since the inconsistency be-

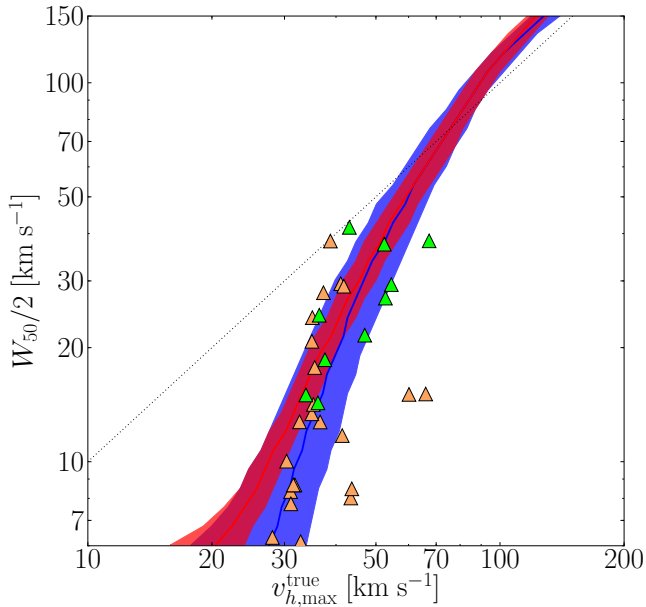


**Fig. 6.** The MORIA dwarfs in the  $W_{50} - v_{h,max}$  plane. Green symbols are the simulations for which we resolved rotation curves are available. The red and blue lines are the P16-relations derived from different observational datasets, with the bands around them representing their uncertainty.

tween the predicted velocity profiles of simulations that are able to reproduce the observational VF, and the measured outermost-point rotational velocities of small dwarfs is at the heart of the TBTF problem (e.g. Papastergis & Ponomareva 2016, see also Trujillo-Gomez et al. 2016; Schneider et al. 2016).

### 3.2. Halo profile fitting

The NFW profile (Navarro et al. 1996) has the form

$$\rho_{\text{NFW}}(R) = \frac{\rho_s}{\left(\frac{R}{R_s}\right) \left(1 + \frac{R}{R_s}\right)^2} \quad (7)$$

and the DC14 profile is given by the expression (Di Cintio et al. 2014)

$$\rho_{\text{DC14}}(R) = \frac{\rho_s}{\left(\frac{R}{R_s}\right)^\gamma \left(1 + \left(\frac{R}{R_s}\right)^\alpha\right)^{(\beta-\gamma)/\alpha}}, \quad (8)$$

where  $R_s$  is scale length and  $\rho_s$  is a multiple of the density at radius  $R = R_s$ . The NFW profile was derived from dark-matter only simulations while the DC14 profile takes the halo response to baryonic effects into account. The  $\alpha$ ,  $\beta$ , and  $\gamma$  parameters are set by the star formation efficiency of the galaxy (quantified by the ratio of stellar to halo mass,  $M_\star/M_h$ ). For  $\alpha = 1$ ,  $\beta = 3$ , and  $\gamma = 1$ , the DC14 profile coincides with the NFW profile. If the stellar mass of the galaxy is known, both profiles have only two free parameters: the halo mass  $M_h$  and the halo concentration  $c = R_{\text{vir}}/R_s$ , with  $R_{\text{vir}}$  the virial radius.

P16 fitted both these profiles to the velocity measured at the outermost H I point of each galaxy (data taken from Begum et al. (2008a); de Blok et al. (2008); Oh et al. (2011); Swaters et al. (2009, 2011); Trachternach et al.

(2009); Kirby et al. (2012); Côté et al. (2000); Verheijen & Sancisi (2001); Sanders (1996); Hunter et al. (2012); Oh et al. (2015); Cannon et al. (2011); Giovanelli et al. (2013); Bernstein-Cooper et al. (2014)). They fixed the halo concentration to the mean cosmic value ( $\log_{10} c = 0.905 - 0.101 \log_{10}(M_h/(10^{12} h^{-1} M_\odot))$ ; Dutton & Macciò 2014), leaving only the halo mass as a free parameter. From the fitted profile, they compute the maximum circular velocity of each galaxy's host halo. In a successful cosmological model, individual galaxies should have  $W_{50} - v_{h,max}^{\text{fit}}$  data-points that agree with the average  $W_{50} - v_{h,max}^{\text{true}}$  relation that is needed to reproduce the observed VF (blue and red bands in Fig. 6). As shown by P16, all is not well: a sizable fraction of low-mass galaxies fall to the left of the expected  $W_{50} - v_{h,max}^{\text{true}}$  relation. In other words: the halo circular velocity implied by their H I kinematics is too low.

We exactly replicate this analysis for the MORIA dwarfs and show the results in Fig. 7. Although there are fewer MORIA dwarfs than in the P16 sample, the result is broadly the same: the  $W_{50} - v_{h,max}^{\text{fit}}$  relation is inconsistent with the expected  $W_{50} - v_{h,max}^{\text{true}}$  relation. Analyzed in this way, one would be driven to the conclusion that the MORIA dwarfs do not follow the  $W_{50} - v_{h,max}^{\text{true}}$  relation required for the  $\Lambda$ CDM halo VF to match the observed galactic VF and, therefore, that they suffer from the TBTF problem. The crucial difference between Fig. 6 and Fig. 7 is the fact that in the former Fig. the maximum halo velocity,  $v_{h,max}^{\text{true}}$ , is computed directly from the enclosed mass profile of each simulated galaxy, while in the latter Fig.  $v_{h,max}^{\text{fit}}$  is computed by fitting the mock H I kinematics of each simulated galaxy.

## 4. Discussion

### 4.1. Does the H I rotation curve trace the potential?

The fact that  $v_{h,max}^{\text{true}}$  and  $v_{h,max}^{\text{fit}}$  have different values, might be explained by an observational effect: the H I rotation curve of dwarf galaxies does not exactly follow the underlying potential.

Indeed, as one can see in Figs. 3 and A.1-A.5, the H I circular velocity profiles ( $v_{\text{circ}}^{\text{obs}}(R)$ ) of the MORIA dwarfs are quite different, even after correcting for pressure support, from the true circular velocity profiles ( $v_{\text{circ}}^{\text{true}}(R)$ ). More often than not, *the outer H I rotation velocity data-point falls significantly below the true value of the local circular velocity*. It is important to keep in mind that the preceding statement is not directly related to the fact that rotational velocities derived from the linewidth of the H I profile of dwarf galaxies,  $W_{50}/2$ , underestimate the maximum circular velocity of the host halo,  $v_{h,max}^{\text{true}}$ , a result that has already been reported by Macciò et al. (2016) and Brooks et al. (2017). In fact, the linewidth derived H I velocity probes radii much smaller than the radius where the host halo rotation curves peaks, and thus there is no guarantee that the two quantities should be the same. What we demonstrate here instead is that the circular velocity computed from spatially resolved H I data underestimates the true circular velocity *at the same radius*. Of course, there are only ten MORIA dwarf galaxies with resolved rotation curves and a bigger sample of simulated dwarfs is definitely needed to fully explore this issue. But if this explanation holds water, it would explain why the halo fitting using a fixed concen-

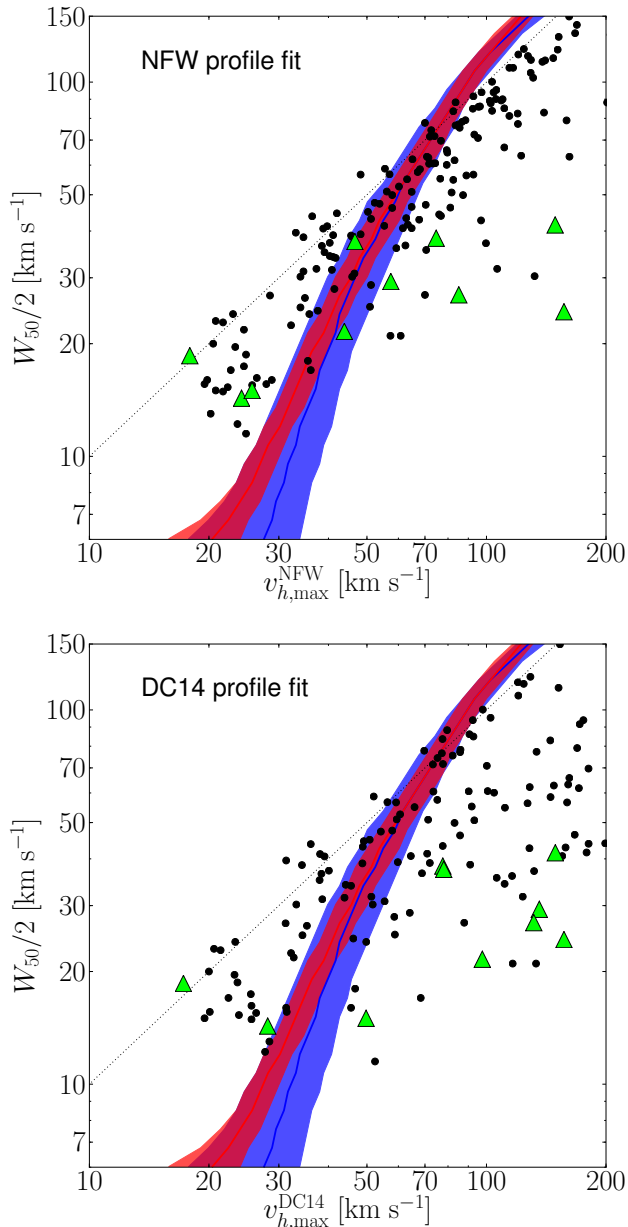


**Fig. 7.** Results from fitting an NFW (top panel) and DC14 (bottom panel) to the outer-most point of the rotation curves of the MORIA simulations using a fixed halo concentration. This is compared to the results from P16 (in black). Red and blue lines and bands are the same as in Fig. 6.

tration fails: we are not fitting to the actual halo velocity at this radius.

In Appendix B, we briefly redo the halo fitting, but now fixing the halo mass using an abundance matching relation and keeping the halo concentration as a free parameter. In short, the resulting concentrations do not seem to be drawn from the distribution predicted by  $\Lambda$ CDM, especially for galaxies with low  $W_{50}$ . If the observed H I rotation curve does not trace the potential, this would explain the seemingly wrong population of concentrations.

Pineda et al. (2017) showed that for galaxies with an idealized set-up, correcting for pressure support fails in the

inner regions due to observational effects. Here, using more realistic dwarf galaxies, we show that the idea that the H I rotation is not necessarily a good tracer for the underlying gravitational potential is not necessarily confined to the inner regions of galaxies.

One crucial question here is what causes this substantial underestimate of the local circular velocity in observational measurements of the H I kinematics. We attribute this to the fact that the assumptions underlying the tilted-ring fitting method and the asymmetric-drift correction are not met in the case of low-mass dwarf galaxies: their atomic ISM simply does not form a relatively flat, dynamically cold disc. Rather, they have a vertically thick ( $\langle q \rangle \sim 0.5$ ), dynamically hot, continuously stirred atomic ISM with significant substructures that is not in dynamical equilibrium in the gravitational potential. The detailed analysis of the vertical structure of the H I disks of MORIA dwarfs and of non-circular motions in their velocity fields will be the focus of a separate publication (Verbeke et al. in prep.)

#### 4.2. Are disturbed velocity fields realistic?

As can be seen from Figs. A.1-A.5, the H I distributions of the MORIA galaxies are generally quite disturbed. This is also the case for real dwarf galaxies with velocity widths  $W_{50}/2 \lesssim 30 \text{ km s}^{-1}$ ; see e.g. Leo P (Bernstein-Cooper et al. 2014), CVndwA, DDO 210, and DDO 216 (Oh et al. 2015). However, examples of real dwarf galaxies with larger velocity widths and regular velocity fields can be found in the literature, (e.g. Kirby et al. 2012). This might indicate too strong an influence of stellar feedback in the more massive MORIA dwarfs, although the spatial (sub)structure of their H I distributions shows no evidence for this. Indeed, the H I sizes and thickness were shown to be in agreement with observed dwarfs in Figs. 1 and 2. On top of that, it was shown in Fig. 9 of V15 that the H I spatial distribution resembles that of real dwarfs by comparing the H I power spectra of MORIA dwarfs to those of LITTLE THINGS (Zhang et al. 2012; Hunter et al. 2012). We leave the investigation of this, including the effect of e.g. beam size, for future research.

In any case, this does not change the conclusions of this paper in any way since these are based on the galaxies with  $W_{50}/2 \lesssim 30 \text{ km s}^{-1}$ .

## 5. Conclusions

We use the MORIA simulations of dwarf galaxies with realistic H I distributions and kinematics to investigate the Too Big To Fail problem for late-type field dwarfs.

We show that the MORIA dwarfs follow the relation between H I line-width and halo circular velocity, derived by Papastergis & Shankar (2016), that is required for the  $\Lambda$ CDM halo velocity function to correspond to the observed field galaxy width function. This means that, given the number density of halos formed in a  $\Lambda$ CDM universe, the MORIA simulations reproduce the observed galactic velocity function. In other words: there is no missing dwarfs in the MORIA simulations.

We then construct resolved H I rotation curves, including asymmetric-drift correction, for ten of the MORIA dwarf galaxies. We use our mock H I rotation curves to replicate the analysis of Papastergis & Shankar (2016) and fit NFW and DC14 density profiles (with fixed concentration parameter) to the outermost point of these measured rotation

curves to derive an observational estimate for the maximum halo circular velocity of each MORIA galaxy. Using this estimate for the circular velocity, the MORIA dwarfs, like the real dwarf galaxies analyzed by Papastergis & Shankar (2016), fail to adhere to the relation between H I line-width and halo circular velocity that is required for the  $\Lambda$ CDM halo velocity function to correspond to the observed field galaxy width function. In other words: using only quantities derived from observations, dwarf galaxies (both real and simulated) experience the Too Big To Fail problem.

What causes this difference between the results from fitting a halo profile to the outer-most point of the rotation curve and using the actual  $v_{h,\max}^{\text{true}}$ -value derived directly from the mass distribution?

Comparing the H I rotation curves of the MORIA dwarf galaxies with their theoretical halo circular velocity curves, we see that they can differ significantly. The circular velocities derived from the H I kinematics of MORIA dwarfs with H I rotation velocities below  $\sim 30 \text{ km s}^{-1}$  are typically too low. This results in too low a  $v_{h,\max}^{\text{fit}}$  value at a fixed concentration  $c$ . The TBTF problem thus results, at least partially, from the fact that for galaxies in this regime, its halo mass can not readily be inferred from its (H I) kinematics. Indeed, based on their kinematics, galaxies with  $W_{50}/2 \lesssim 30 \text{ km s}^{-1}$  would seem to inhabit less massive halos than they actually do. However, under the assumptions of  $\Lambda$ CDM, the P16-relation does provide an estimate of the true halo circular velocity  $v_{h,\max}^{\text{true}}$  in function of a galaxies H I linewidth  $W_{50}$ .

We attribute this effect to that fact that the atomic interstellar medium of low-mass dwarfs simply does not form a relatively flat, dynamically cold disc whose kinematics directly traces the underlying gravitational force field. Another explanation might be that the H I velocity fields are too irregular to infer its halo mass from its kinematics. This is true for most of the simulated galaxies presented in this work, as well as for observed low-mass galaxies.

The stellar feedback efficiency will influence both these H I-thickness of the galaxies as well as how messy the velocity fields are. Thus, how much energy is actually injected in the ISM by stellar feedback is an important issue in the discussion of the Too Big To Fail problem.

## Acknowledgements

This research has been funded by the Interuniversity Attraction Poles Programme initiated by the Belgian Science Policy Office (IAP P7/08 CHARM). EP is supported by a NOVA postdoctoral fellowship of the Netherlands Research School for Astronomy (NOVA). SDR thanks the Ghent University Special Research Fund (BOF) for financial support. We thank Flor Allaert, Antonino Marasco, and Arianna Di Cintio for useful discussions. We thank Volker Springel for making the GADGET-2 simulation code publicly available.

## References

Begeman, K. G. 1989, *A&A*, 223, 47  
 Begum, A., Chengalur, J. N., Karachentsev, I. D., & Sharina, M. E. 2008a, *MNRAS*, 386, 138  
 Begum, A., Chengalur, J. N., Karachentsev, I. D., Sharina, M. E., & Kaisin, S. S. 2008b, *MNRAS*, 386, 1667  
 Behroozi, P. S., Wechsler, R. H., & Conroy, C. 2013, *ApJ*, 770, 57  
 Bernstein-Cooper, E. Z., Cannon, J. M., Elson, E. C., et al. 2014, *AJ*, 148, 35

Boylan-Kolchin, M., Bullock, J. S., & Kaplinghat, M. 2011, *MNRAS*, 415, L40  
 Boylan-Kolchin, M., Bullock, J. S., & Kaplinghat, M. 2012, *MNRAS*, 422, 1203  
 Brook, C. B. & Di Cintio, A. 2015, *MNRAS*, 450, 3920  
 Brooks, A. M., Papastergis, E., Christensen, C. R., et al. 2017, *ArXiv e-prints*  
 Brooks, A. M. & Zolotov, A. 2014, *ApJ*, 786, 87  
 Cai, R.-G., Guo, Z.-K., & Tang, B. 2014, *Phys. Rev. D*, 89, 123518  
 Cannon, J. M., Giovanelli, R., Haynes, M. P., et al. 2011, *ApJ*, 739, L22  
 Christensen, C. R., Governato, F., Quinn, T., et al. 2014, *MNRAS*, 440, 2843  
 Cloet-Osselaer, A., De Rijcke, S., Vandenbroucke, B., et al. 2014, *MNRAS*, 442, 2909  
 Côté, S., Carignan, C., & Freeman, K. C. 2000, *AJ*, 120, 3027  
 de Blok, W. J. G., Walter, F., Brinks, E., et al. 2008, *AJ*, 136, 2648  
 De Rijcke, S., Schroyen, J., Vandenbroucke, B., et al. 2013, *MNRAS*, 433, 3005  
 Di Cintio, A., Brook, C. B., Dutton, A. A., et al. 2014, *MNRAS*, 441, 2986  
 Di Teodoro, E. M. & Fraternali, F. 2015, 3D-Barolo: 3D fitting tool for the kinematics of galaxies, *Astrophysics Source Code Library*  
 Dutton, A. A. & Macciò, A. V. 2014, *MNRAS*, 441, 3359  
 Ferrero, I., Abadi, M. G., Navarro, J. F., Sales, L. V., & Gurovich, S. 2012, *MNRAS*, 425, 2817  
 Garrison-Kimmel, S., Boylan-Kolchin, M., Bullock, J. S., & Kirby, E. N. 2014, *MNRAS*, 444, 222  
 Giovanelli, R., Haynes, M. P., Adams, E. A. K., et al. 2013, *AJ*, 146, 15  
 Governato, F., Zolotov, A., Pontzen, A., et al. 2012, *MNRAS*, 422, 1231  
 Guo, Q., White, S., Li, C., & Boylan-Kolchin, M. 2010, *MNRAS*, 404, 1111  
 Haynes, M. P., Giovanelli, R., Martin, A. M., et al. 2011, *AJ*, 142, 170  
 Hunter, D. A., Ficut-Vicas, D., Ashley, T., et al. 2012, *AJ*, 144, 134  
 Iorio, G., Fraternali, F., Nipoti, C., et al. 2016, *ArXiv e-prints*  
 Katz, H., Lelli, F., McGaugh, S. S., et al. 2017, *MNRAS*, 466, 1648  
 Kirby, E. M., Koribalski, B., Jerjen, H., & López-Sánchez, Á. 2012, *MNRAS*, 420, 2924  
 Klypin, A., Karachentsev, I., Makarov, D., & Nasonova, O. 2015, *MNRAS*, 454, 1798  
 Lelli, F., McGaugh, S. S., & Schombert, J. M. 2016, *AJ*, 152, 157  
 Lelli, F., Verheijen, M., Fraternali, F., & Sancisi, R. 2012, *A&A*, 544, A145  
 Macciò, A. V., Udrescu, S. M., Dutton, A. A., et al. 2016, *MNRAS*, 463, L69  
 Mamon, A. A., Bamba, K., & Das, S. 2017, *European Physical Journal C*, 77, 29  
 Moster, B. P., Naab, T., & White, S. D. M. 2013, *MNRAS*, 428, 3121  
 Navarro, J. F., Frenk, C. S., & White, S. D. M. 1996, *ApJ*, 462, 563  
 Oh, S.-H., de Blok, W. J. G., Brinks, E., Walter, F., & Kennicutt, Jr., R. C. 2011, *AJ*, 141, 193  
 Oh, S.-H., Hunter, D. A., Brinks, E., et al. 2015, *AJ*, 149, 180  
 Papastergis, E., Giovanelli, R., Haynes, M. P., & Shankar, F. 2015, *A&A*, 574, A113  
 Papastergis, E. & Ponomareva, A. A. 2016, *ArXiv e-prints*  
 Papastergis, E. & Shankar, F. 2016, *A&A*, 591, A58  
 Pineda, J. C. B., Hayward, C. C., Springel, V., & Mendes de Oliveira, C. 2017, *MNRAS*, 466, 63  
 Planck Collaboration, Ade, P. A. R., Aghanim, N., et al. 2016, *A&A*, 594, A13  
 Read, J. I., Agertz, O., & Collins, M. L. M. 2016, *MNRAS*, 459, 2573  
 Read, J. I., Iorio, G., Agertz, O., & Fraternali, F. 2017, *MNRAS*  
 Rodríguez-Puebla, A., Behroozi, P., Primack, J., et al. 2016, *MNRAS*, 462, 893  
 Roychowdhury, S., Chengalur, J. N., Begum, A., & Karachentsev, I. D. 2010, *MNRAS*, 404, L60  
 Sales, L. V., Navarro, J. F., Oman, K., et al. 2017, *MNRAS*, 464, 2419  
 Sanders, R. H. 1996, *ApJ*, 473, 117  
 Sawala, T., Frenk, C. S., Fattahi, A., et al. 2015, *MNRAS*, 448, 2941  
 Sawala, T., Frenk, C. S., Fattahi, A., et al. 2016, *MNRAS*, 456, 85  
 Schneider, A., Trujillo-Gomez, S., Papastergis, E., Reed, D. S., & Lake, G. 2016, *ArXiv e-prints*  
 Suzuki, N., Rubin, D., Lidman, C., et al. 2012, *ApJ*, 746, 85  
 Swaters, R. A., Sancisi, R., van Albada, T. S., & van der Hulst, J. M. 2009, *A&A*, 493, 871  
 Swaters, R. A., Sancisi, R., van Albada, T. S., & van der Hulst, J. M. 2011, *ApJ*, 729, 118

- Tollerud, E. J., Boylan-Kolchin, M., & Bullock, J. S. 2014, MNRAS, 440, 3511
- Trachternach, C., de Blok, W. J. G., McGaugh, S. S., van der Hulst, J. M., & Dettmar, R.-J. 2009, A&A, 505, 577
- Trujillo-Gomez, S., Schneider, A., Papastergis, E., Reed, D. S., & Lake, G. 2016, ArXiv e-prints
- van der Hulst, J. M., Terlouw, J. P., Begeman, K. G., Zwitter, W., & Roelfsema, P. R. 1992, in Astronomical Society of the Pacific Conference Series, Vol. 25, Astronomical Data Analysis Software and Systems I, ed. D. M. Worrall, C. Biemesderfer, & J. Barnes, 131
- Verbeke, R., Vandenbroucke, B., & De Rijcke, S. 2015, ApJ, 815, 85
- Verheijen, M. A. W. & Sancisi, R. 2001, A&A, 370, 765
- Wang, J., Frenk, C. S., Navarro, J. F., Gao, L., & Sawala, T. 2012, MNRAS, 424, 2715
- Wang, L., Dutton, A. A., Stinson, G. S., et al. 2015, MNRAS, 454, 83
- Zhang, H.-X., Hunter, D. A., & Elmegreen, B. G. 2012, ApJ, 754, 29

## Appendix A: H I catalogue

A synthetic observation of one our simulations was already presented in Fig. 3. Here, the rest of the MORIA simulations discussed in this paper are shown in Figs. A.1-A.5.

## Appendix B: Concentration fitting

To be able to fit the two-parameter density profiles given by eqns. (7) and (8) to only two points (the central and outermost measured point of the rotation curve), P16 kept the concentration  $c$  of the halos fixed at the mean cosmic value and used the halo mass  $M_h$  as a free parameter. Another choice would be to fix  $M_h$  using the stellar mass and an abundance matching relation and to keep the concentration  $c$  as a free parameter.

In Fig. B.1, we show the  $W_{50} - v_{h,max}^{fit}$  relation obtained by fitting NFW and DC14 profiles to the P16 dataset, using the concentration  $c$  as a free parameter with the halo mass  $M_h$  set by the stellar mass and the Moster et al. (2013) abundance matching relation. This way, the observed galaxies adhere much more closely to the expected  $W_{50} - v_{h,max}^{true}$  relation. NFW and DC14 profiles now actually produce very similar results.

In Fig. B.2, we compare the concentrations of the P16 galaxies retrieved in this way with the mass-dependent cosmic mean value derived from cosmological simulations (Dutton & Macciò 2014). The frequency distribution of the concentration values is well approximated with a log-normal distribution function. Both for an NFW and a DC14 fit, the scatter is  $\sigma \approx 0.25 - 0.3$  dex. This is significantly larger than the scatter on  $\log(c/\langle c \rangle)$  found in cosmological simulations, where  $\sigma \sim 0.13$  (Dutton & Macciò 2014).

In Fig. B.2, we distinguish between galaxies with  $W_{50}/2 < 30 \text{ km s}^{-1}$  (red data-points) and  $W_{50}/2 > 30 \text{ km s}^{-1}$  (blue data-points), for the fits with the NFW and DC14 profiles. We choose the  $30 \text{ km s}^{-1}$  split because this is the rotation velocity below which the TBTF problem becomes apparent. Clearly, the high- $W_{50}$  galaxies have higher concentrations than expected while the low- $W_{50}$  dwarfs have lower concentrations, with a hint of an anticorrelation between  $M_h$  and concentration for the low  $W_{50}$  galaxies. This is to be expected: higher-mass galaxies must have lower concentrations in order to have low circular velocities. To see whether the average of each subsample differs significantly from the cosmic mean value, we ran a  $t$ -test on both populations. We find  $p$ -values of 0.025 and  $4.2 \times 10^{-8}$  for the galaxies with respectively high and low  $W_{50}$ . The full sample has a mean concentration consistent with the Dutton

& Macciò (2014) simulations, unlike the subsamples separately. For the DC14 profile, the same trend is found, with all the averages slightly higher than for the NFW profile. The  $p$ -values for the  $t$ -test are  $2.0 \times 10^{-7}$  for the entire sample and  $1.3 \times 10^{-10}$  and 0.0047 for the high and low circular velocity samples respectively. Employing the DC14 density profile yields concentration estimates that are inconsistent with the Dutton & Macciò (2014) simulations, both for the full sample and the subsamples.

Both the large scatter and the offsets are probably due, at least in part, to uncertainties on the (extrapolated) low-mass end of the  $M_\star - M_h$  relation that was used to derive the halo mass from the stellar mass. In the mass regime we are interested in, the scatter on the  $M_\star - M_h$  relation is expected to be substantial (e.g. Sales et al. 2017) and, using our approach, this translates in an increased scatter on the concentration parameter. Moreover, there is great variation among the different published  $M_\star - M_h$  relations in the regime of dwarf galaxies ( $M_h \approx 10^{10} M_\odot$ ). Simulations also show a large scatter in stellar mass for these type of halos (e.g. Fig. 7 in V15). We redid our analysis adopting different  $M_\star - M_h$  relations: using the relation of Guo et al. (2010), we reach the same conclusions as for the relation of Moster et al. (2013); when using the relation of Behroozi et al. (2013), the fitted concentrations are more in line with the predictions from  $\Lambda$ CDM, however they do not follow the P16-relation.

Katz et al. (2017) fitted an NFW and a DC14-profile to 147 SPARC-galaxies, taken from a sample of 175 galaxies with extended H I rotation curves (Lelli et al. 2016). They conclude that the fitted halo masses and concentrations for the DC14-profile are in line with the predictions from  $\Lambda$ CDM. The difference with our results is that their conclusions is that they only discuss their entire sample, which consists mostly of high-mass galaxies. They also use full rotation curves to fit the halo profile to the galaxies, allowing them to fit the halo mass and concentration simultaneously.

By fitting a *coreNFW* profile (Read et al. 2016) to full rotation curves of a subset of the Little THINGS galaxies (Iorio et al. 2016), Read et al. (2017) find that these isolated dwarf galaxies inhabit halos consistent with the abundance matching relation of Behroozi et al. (2013) and, as such, do not find a TBTF for isolated galaxies *at all*. These conclusions would change when assuming a different  $M_\star - M_{halo}$  relation, as they remark in their Appendix C. Even so, we still find that using the relation of Behroozi et al. (2013), the observations do not follow the P16-relation.



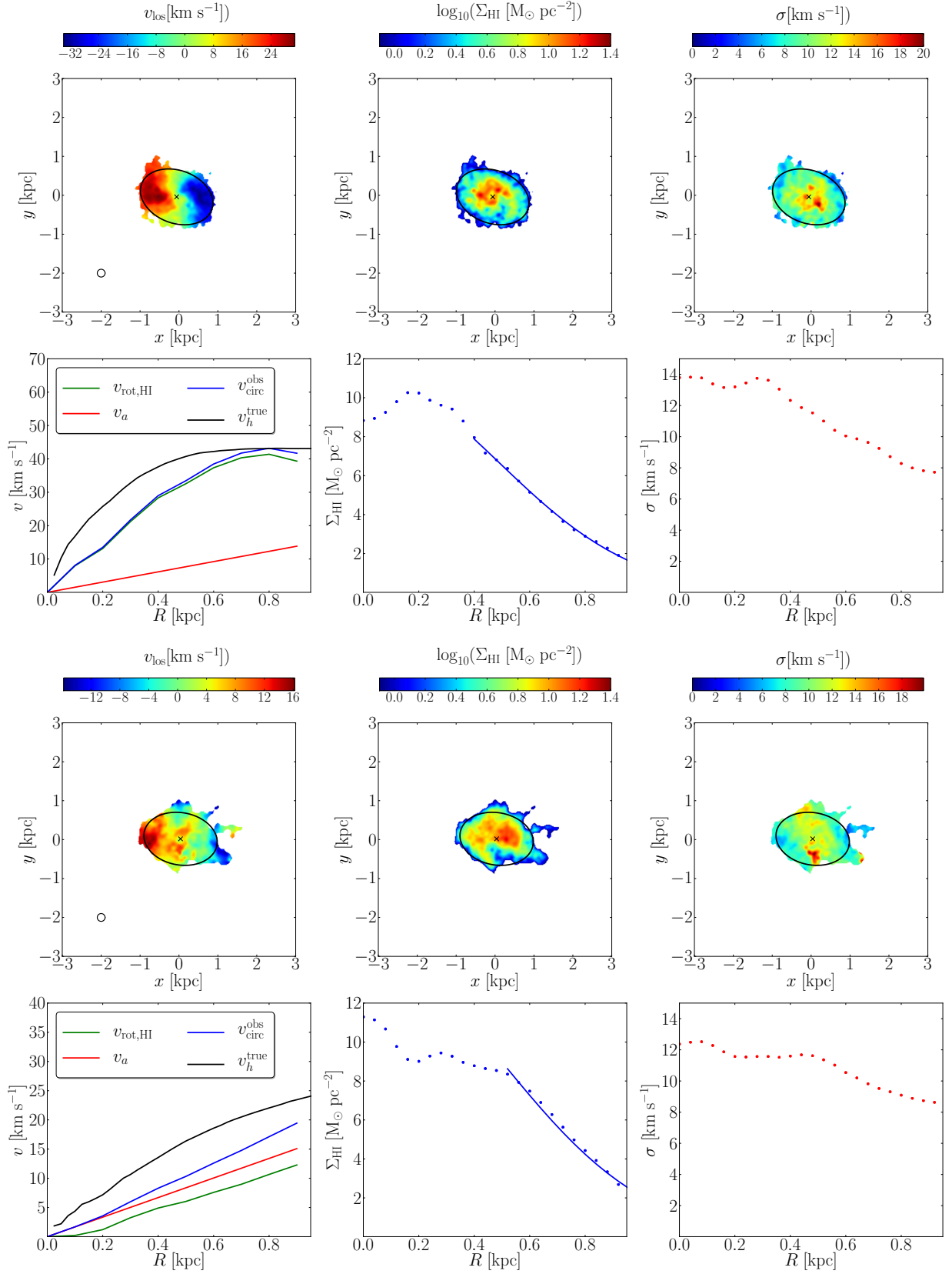


**Fig. A.1.** Same as in Fig. 3.

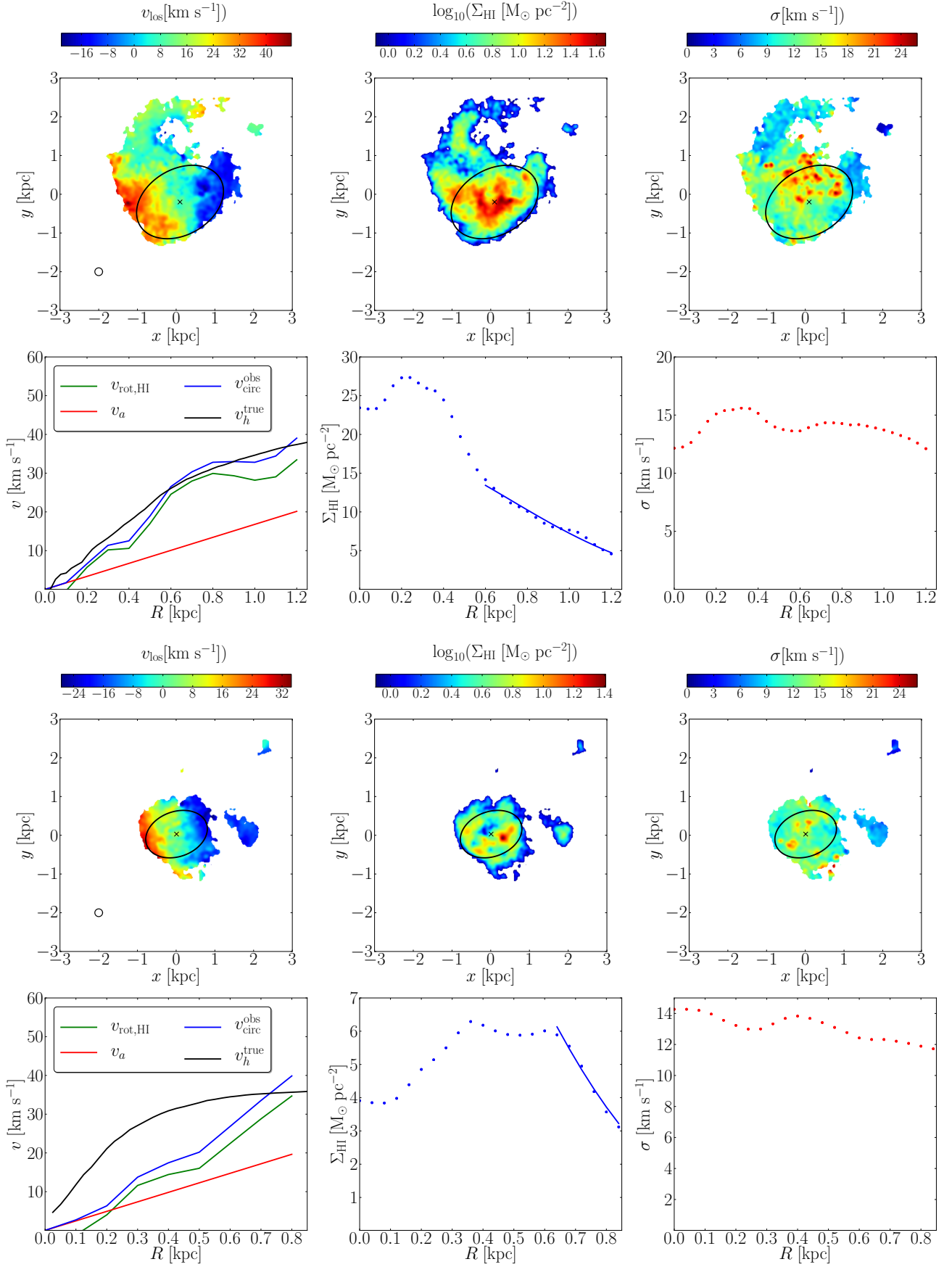
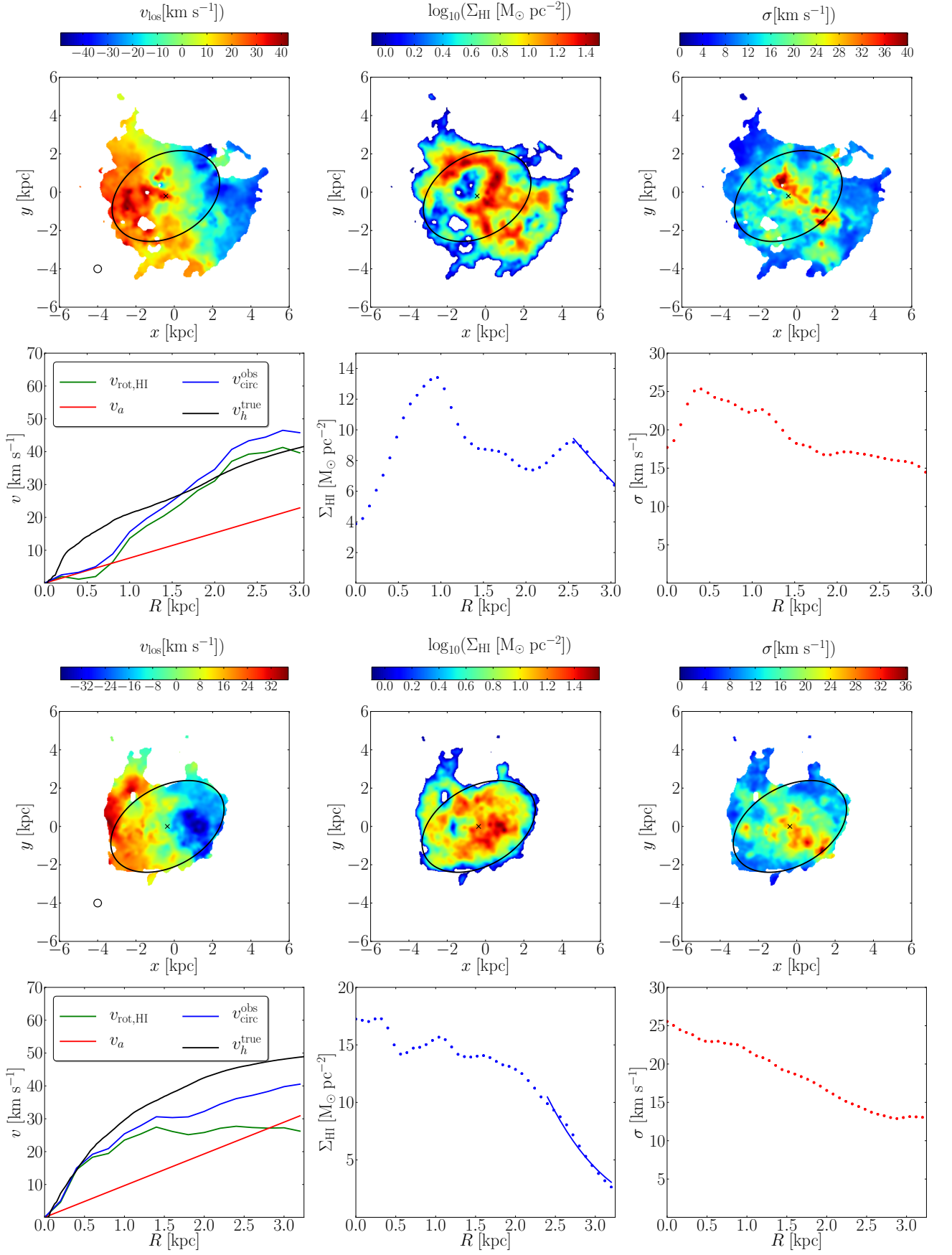


Fig. A.2. Same as in Fig. 3.





**Fig. A.3.** Same as in Fig. 3.

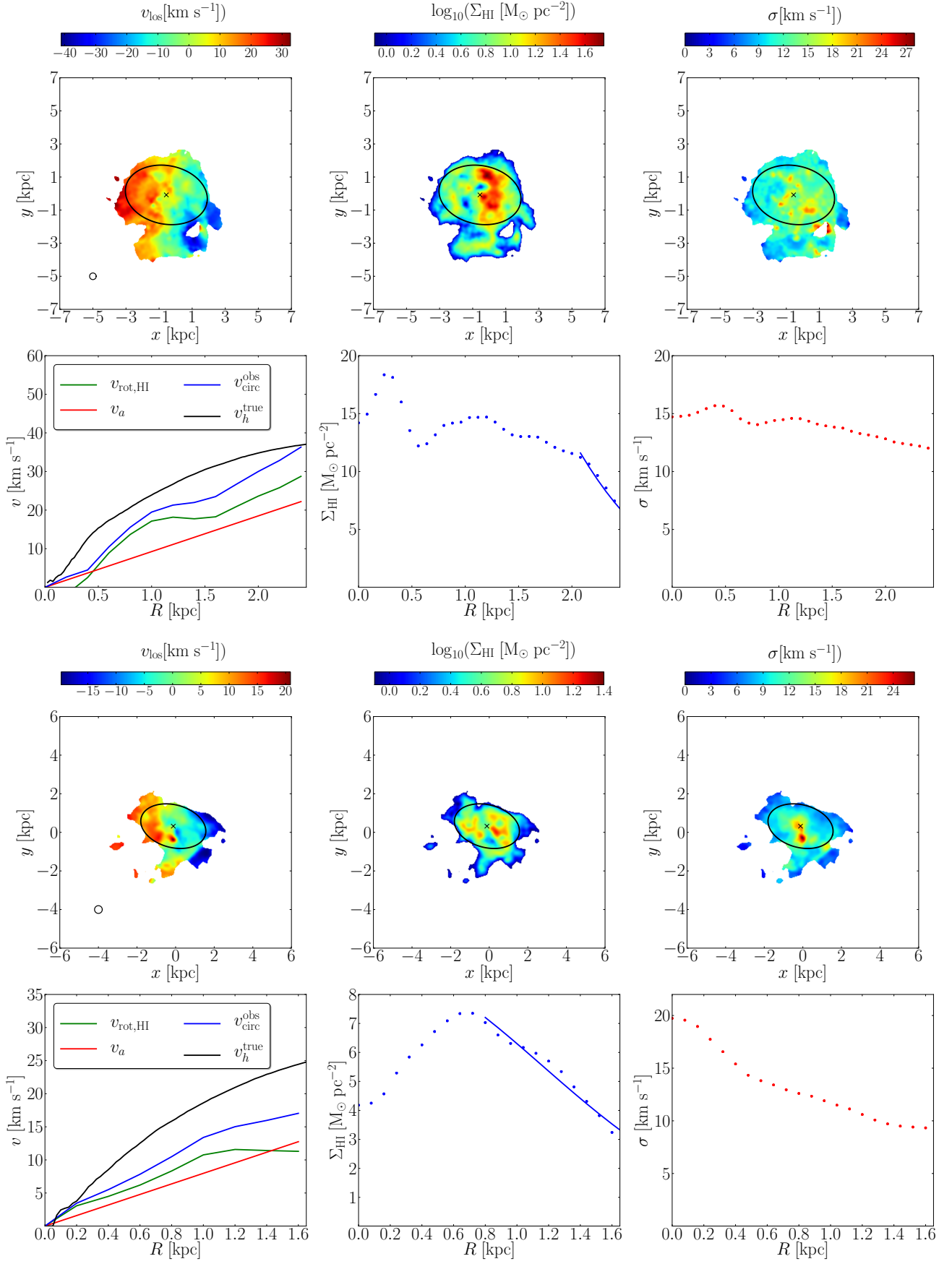
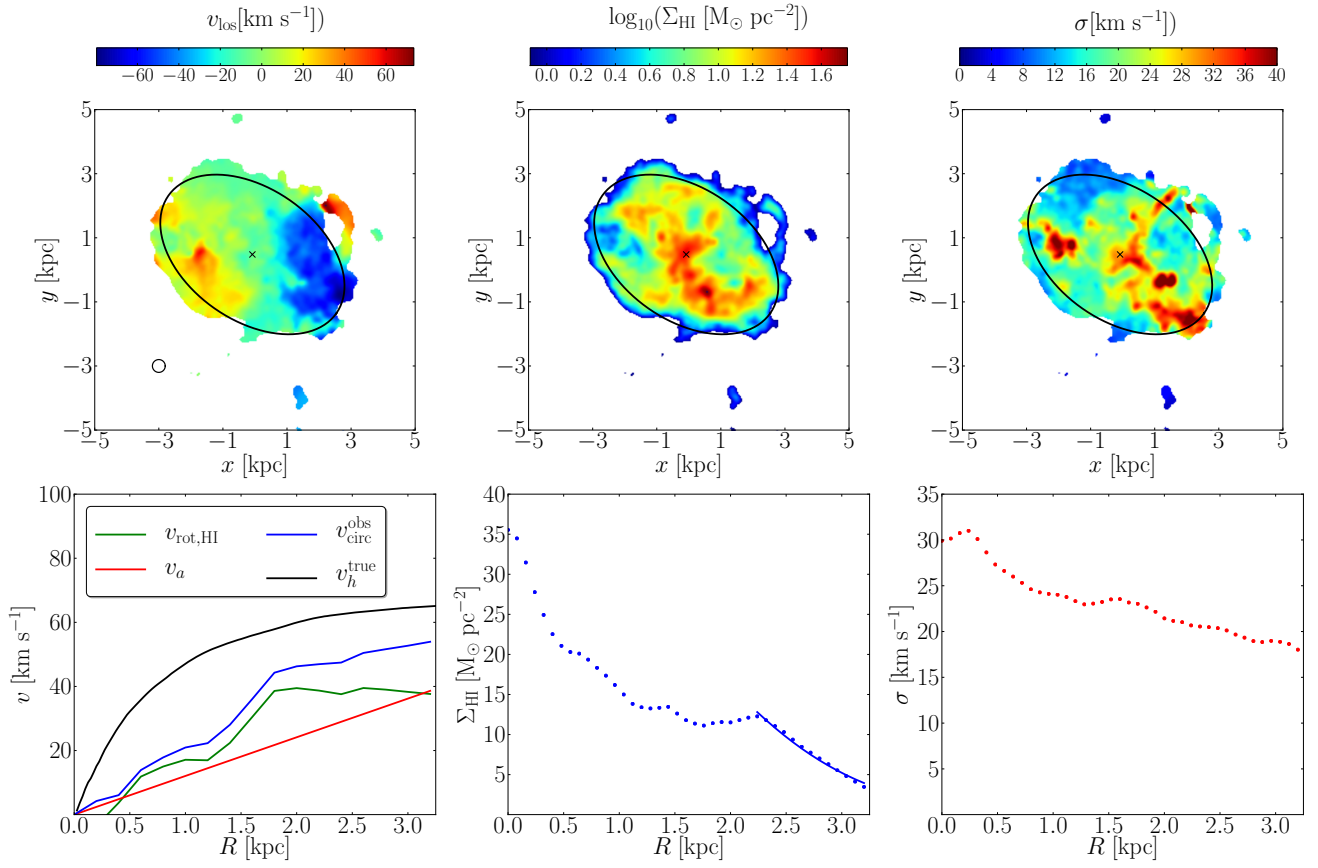
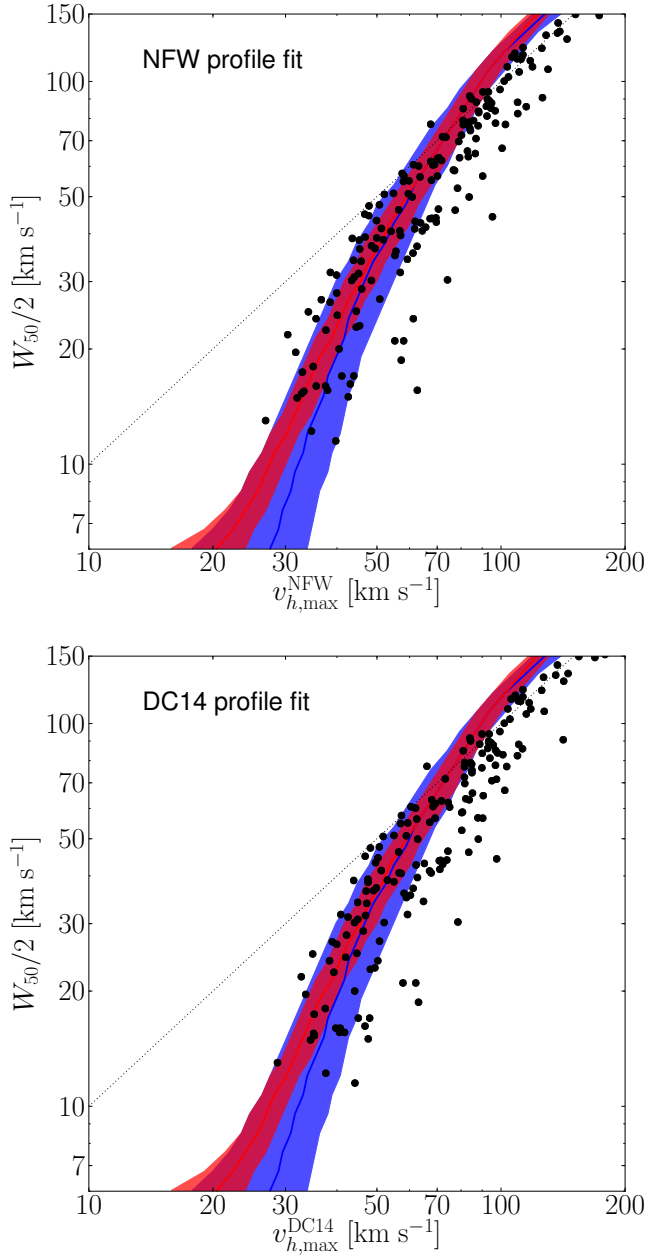


Fig. A.4. Same as in Fig. 3.



**Fig. A.5.** Same as in Fig. 3.



**Fig. B.1.** Results from fitting an NFW (top panel) and DC14 (bottom panel) to the outer-most point of the rotation curves of the observations used in Papastergis & Shankar (2016) using a fixed halo mass, keeping the halo concentration as a free parameter. The halo mass is calculated from their stellar mass using the abundance matching relation of Moster et al. (2013). Red and blue lines and bands are the same as in Fig. 7.

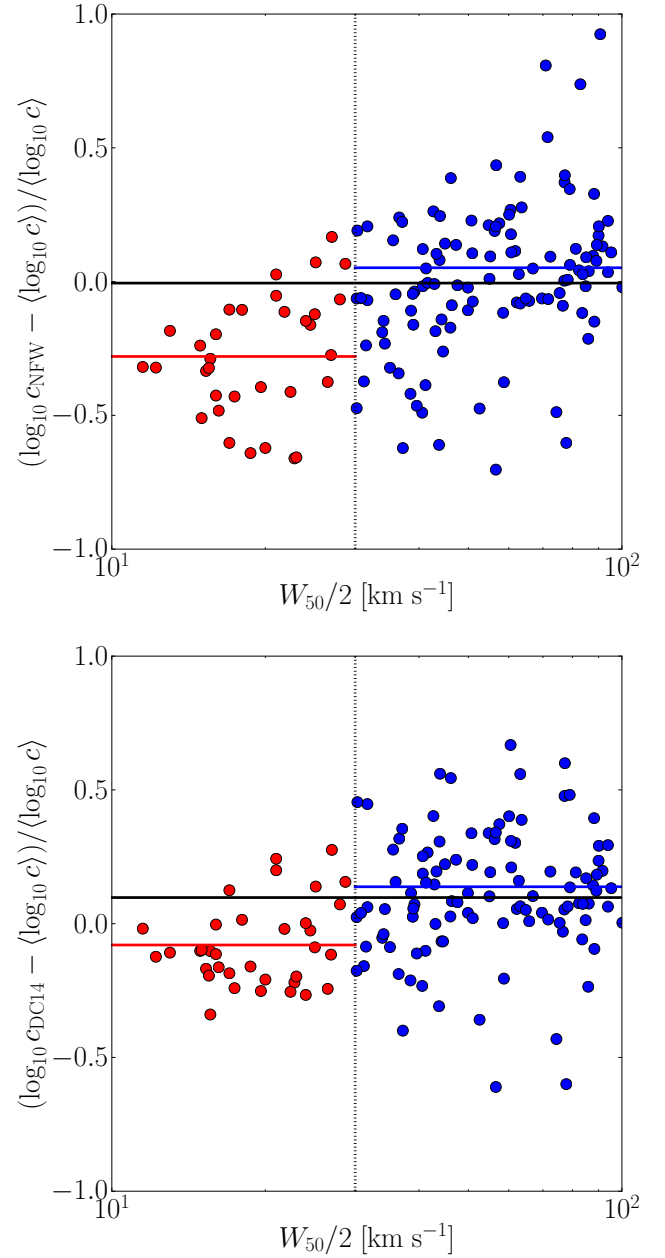


**Fig. B.2.** Logarithmic difference between the fitted concentration and the one expected from cosmological dark-matter only simulations (Dutton & Macciò 2014) of the P16 sample of galaxies. Top panel: concentration obtained by fitting the NFW density profile to the kinematic data; bottom panel: concentration obtained using the DC14 density profile. Red and blue symbols indicate galaxies with low and high H I rotation velocities, respectively. The red and blue lines indicate the mean concentration of both subsamples; the green line indicates the mean concentration of the full sample.